12-28-2012

An Investigation of Oxygen Reduction Kinetics in LSF Electrodes

Rainer Küngas
University of Pennsylvania

Anthony S. Yu
University of Pennsylvania

Julie Levine
University of Pennsylvania

John M. Vohs
University of Pennsylvania, vohs@seas.upenn.edu

Raymond J. Gorte
University of Pennsylvania, gorte@seas.upenn.edu

Küngas, R., Yu, A. S., Levine, J., Vohs, J. M., Gorte, R. J. (2012). An Investigation of Oxygen Reduction Kinetics in LSF Electrodes. *Journal of the Electrochemical Society, 160*(2), F205-F211. doi: 10.1149/2.011303jes

An Investigation of Oxygen Reduction Kinetics in LSF Electrodes

Abstract
The characteristics of solid oxide fuel cell (SOFC) cathodes, prepared by infiltration of $La_{0.8}Sr_{0.2}FeO_{3-\delta}$ (LSF) into porous yttria-stabilized zirconia (YSZ) scaffolds, were evaluated by studying the effect of $p(O_2)$ and of Al_2O_3overlayers deposited by Atomic Layer Deposition (ALD) on impedance spectra at 873 and 973 K. The electrode resistance of LSF-YSZ composites calcined at 1123 K was dominated by high-frequency processes that show a relatively weak $p(O_2)$ dependence of −0.2 at 973 K. Composites calcined to 1373 K exhibited additional, low-frequency features in their impedance spectra that were more strongly dependent on $p(O_2)$, −0.43. These low-frequency processes are due to O_2 adsorption limitations caused by the lower surface area of the LSF phase. Decreases in the exposed LSF surface caused by ALD films caused similar changes in the impedance spectra. The ALD overlayers were disrupted by heating to 1073 K and electrode polarization at 873 K. The implications of these results for understanding O_2 adsorption limitations on SOFC cathodes are discussed.

Disciplines
Chemical Engineering

Comments
Küngas, R., Yu, A. S., Levine, J., Vohs, J. M., Gorte, R. J. (2012). An Investigation of Oxygen Reduction Kinetics in LSF Electrodes. *Journal of the Electrochemical Society, 160*(2), F205-F211. doi: 10.1149/2.011303jes

Journal of The Electrochemical Society, **160** (2) F205-F211 (2013)
0013-4651/2013/160(2)/F205/7/$28.00 © The Electrochemical Society

An Investigation of Oxygen Reduction Kinetics in LSF Electrodes

Rainer Küngas,[*,z] Anthony S. Yu, Julie Levine, John M. Vohs,[**] and Raymond J. Gorte[**]

Department of Chemical and Biomolecular Engineering, University of Pennsylvania, Philadelphia, Pennsylvania 19104, USA

The characteristics of solid oxide fuel cell (SOFC) cathodes, prepared by infiltration of $La_{0.8}Sr_{0.2}FeO_{3-\delta}$ (LSF) into porous yttria-stabilized zirconia (YSZ) scaffolds, were evaluated by studying the effect of $p(O_2)$ and of Al_2O_3 overlayers deposited by Atomic Layer Deposition (ALD) on impedance spectra at 873 and 973 K. The electrode resistance of LSF-YSZ composites calcined at 1123 K was dominated by high-frequency processes that show a relatively weak $p(O_2)$ dependence of −0.2 at 973 K. Composites calcined to 1373 K exhibited additional, low-frequency features in their impedance spectra that were more strongly dependent on $p(O_2)$, −0.43. These low-frequency processes are due to O_2 adsorption limitations caused by the lower surface area of the LSF phase. Decreases in the exposed LSF surface caused by ALD films caused similar changes in the impedance spectra. The ALD overlayers were disrupted by heating to 1073 K and electrode polarization at 873 K. The implications of these results for understanding O_2 adsorption limitations on SOFC cathodes are discussed.
 [DOI: 10.1149/2.011303jes]

Manuscript submitted October 15, 2012; revised manuscript received December 10, 2012. Published December 28, 2012. This was Paper 441 presented at the Seattle, Washington, Meeting of the Society, May 6–10, 2012.

Solid oxide fuel cells (SOFC) can convert any combustible fuel directly into electricity through electrochemical oxidation reactions, thereby providing very high electrical efficiencies.[1–3] The factor limiting overall performance of SOFCs is often the slow oxygen reduction kinetics on the fuel cell cathode, especially for operation at lower temperatures ($T \leq 1073$ K). While Sr-doped $LaMnO_3$ (LSM) based cathodes are still widely used, significantly lower cathode overpotentials can be achieved with alternative perovskite materials, such as Sr-doped $LaFeO_3$ (LSF), $LaCoO_3$ (LSCo), or $LaCo_{1-y}Fe_yO_3$ (LSCF). In addition to having high electronic conductivities (e.g. 80 S/cm for $La_{0.8}Sr_{0.2}FeO_3$ at 973 K in air[4]), these materials possess significant oxygen-ion conductivities ($8.3 \cdot 10^{-4}$ S/cm for $La_{0.8}Sr_{0.2}FeO_3$ at 973 K in air[4]), which extends the active region in the electrode from the immediate vicinity of the three-phase boundary (TPB) region further across the perovskite surface.[3,5,6]

However, there is evidence that the rate-limiting step in composite cathodes based on these mixed conductors is the oxygen reduction reaction at the surface and not oxygen-ion diffusion through the perovskite phase.[3–5,7–15] For example, Bidrawn et al. demonstrated that the performance of cathodes prepared by infiltration of $La_{0.8}Sr_{0.2}FeO_3$ (LSF), $La_{0.8}Ca_{0.2}FeO_3$, or $La_{0.8}Ba_{0.2}FeO_3$ into porous yttria-stabilized zirconia (YSZ) was identical at 973 K despite the fact that the ionic conductivities of these materials vary by a factor of 30.[4] Additional evidence that a surface process limits cathode performance comes from the strong dependence of cell impedance on the surface area of the perovskite phase of the composite cathode[4] and by the fact that cathode performance can be enhanced by the addition of various promoters onto the surface of the electrodes.[7,9,16–24] Finally, a number of mathematical models have stressed the importance of maximizing the electrode active area[7,8,25,26] and point to the adsorption of molecular oxygen on a perovskite vacancy site as the most probable rate-limiting step.[7,8,10]

Despite a large amount of work aimed at characterizing the oxygen-reduction reaction on various materials, there is still much that is not known about the reaction or how to promote it. Characterization of oxygen reduction on working electrodes can be particularly difficult because high performance SOFC cathodes are usually composites of the conductive perovskite and the electrolyte material (e.g. YSZ) and have a relatively complex structure. To simplify the study of SOFC cathodes, our research group has focused on composite cathodes prepared by infiltration of the perovskite into a porous scaffold of the electrolyte.[3,4,7–9,27–33] One of the advantages of preparing electrodes by infiltration is that the electrolyte scaffold can be calcined separately at very high temperatures, prior to the addition of the perovskite, so that the structure of the electrolyte phase can be fixed independently from that of the perovskite phase. Of the various perovskites that are of interest, our group has focused on LSF because it does not react with YSZ at temperatures below 1373 K,[27,28] allowing changes in perovskite microstructure to be examined by varying the calcination temperature of the electrode after infiltration.[3,4,27–33] Past work has shown that high calcination temperatures (e.g. 1373 K) dramatically decrease the surface area of the LSF phase and lead to a significant increase in the non-ohmic electrode resistance at open circuit.[4,7–9,27,28,31–34] It is important to point out that due to the relatively simple microstructure, the electrochemical characteristics of infiltrated SOFC cathodes can be described in terms of mathematical models with no or very few fitting parameters.[7,8,25,26] The electrode kinetics do not exhibit Tafelian behavior and the oxygen reduction reactions should not be described in terms of Butler-Volmer kinetics.[7,8,35]

In the present work, we have examined the oxygen-reduction reaction on an LSF-YSZ cathode by measuring the electrode performances using two different approaches. First, we have examined the impedance spectra as a function of $p(O_2)$ on composites that have been calcined at either high (1373 K) or low (1123 K) temperatures. The $p(O_2)$ dependences were distinctly different for these two cases, indicating that there is a different rate-limiting step. Second, we have used Atomic Layer Deposition (ALD) of Al_2O_3 to form inert blocking layers that partially cover the electrode surface. Because ALD involves a reaction between the film precursor and the surface, submonolayer to multilayer, conformal Al_2O_3 films could be deposited over the electrode surface, so that the electrode impedance could be measured as a function of the fraction of the surface that was covered. The results for LSF-YSZ electrodes that had been calcined at 1123 K and then partially covered with Al_2O_3 were found to be very similar to those for electrodes calcined at higher temperatures without the addition of Al_2O_3. This suggests that the effects on electrode performance due to changes in the LSF surface area are similar whether that change in area results from increased calcination temperature or to blocking of the area by inert species. Additionally, it is shown that polarization irreversibly disrupted the Al_2O_3 film, demonstrating that the cathode surface must undergo restructuring upon polarization.

Experimental

Cell preparation and characterization.— All of the electrochemical measurements in this study were performed using symmetric cells in which the electrodes were prepared by infiltration of nitrate solutions into a porous electrolyte matrix. The first step in cell preparation involved the fabrication of a porous-dense-porous structure of the YSZ electrolyte using tape-casting methods. The tapes for the porous YSZ were prepared by mixing 8 mol.% YSZ powder (Tosoh), a solvent mixture (ethanol and xylenes, Sigma Aldrich), dispersant (Menhaden

*Electrochemical Society Student Member.
**Electrochemical Society Active Member.
zE-mail: kungas@seas.upenn.edu

Fish Oil, Richard Mistler, Inc.), binder (PVB B98, Richard Mistler, Inc.), plasticizers (benzyl butyl phthalate and polyethylene glycol MW = 400, both from Sigma Aldrich), and a pore former (synthetic graphite (300 mesh, Alfa Aesar) and rice starch (Sigma Aldrich) in a weight ratio of 1:2). A detailed description of the tape-casting and lamination procedure is available elsewhere.[29,31,32] The resulting slurry was tape cast and then laminated onto both sides of a YSZ green tape that did not contain pore formers. After sintering at 1773 K for 4 hours, the middle YSZ layer became dense and the porous YSZ scaffolds remained 65–70% porous with a surface area of 0.48 m^2/g. The thicknesses of the dense and porous layers were 80 and 40 μm, respectively.

LSF was introduced into the porous YSZ scaffolds by infiltration with an aqueous solution consisting of $La(NO_3)_3 \cdot 6\,H_2O$ (Alfa Aesar, 99.9%), $Sr(NO_3)_2$ (Alfa Aesar, 99%), and $Fe(NO_3)_3 \cdot 6\,H_2O$ (Fisher Scientific, 98.4%) at a molar ratio of La:Sr:Fe = 0.8:0.2:1.[7,9,27,28,32] Citric acid, in a 1:1 ratio with the metal cations, was used as a complexing agent in order to assist the formation of the perovskite phase at lower temperatures.[29] Infiltration steps were followed by a 0.5-h heat-treatment at 723 K to decompose the nitrates. This procedure was repeated until a loading of 35-wt% LSF was achieved. The composites were then calcined to either 1123 K or to 1373 K for 4 hours. The characteristics of LSF-YSZ electrodes prepared by these methods have been described in detail in other publications.[7–9,27,31–33]

Electrochemical impedance spectra of the symmetric cells were recorded using a Gamry Instruments potentiostat in the frequency range of 0.01 Hz to 300 kHz. All symmetric cell impedances have been divided by two to account for there being two identical electrodes. Silver wires (Strem Chemicals) were attached to both sides of the symmetrical cell with silver paste (SPI Supplies) for current collection, as in earlier publications from our group.[3,4,7–9,28,29,32–34] All measurements were conducted in a two-electrode setup; no reference electrode was used. The effect of oxygen partial pressure on electrode performance was studied by mixing O_2 (99.8%, Airgas) and N_2 (99.999%, Airgas) in the desired ratios. Ambient air and 5% O_2 in Ar mixture (Airgas) were used as reference for $p(O_2) = 0.21$ atm and $p(O_2) = 0.05$ atm. The sample was allowed to equilibrate for 15 minutes in each atmosphere before impedance measurements were conducted.

Electrode modification by ALD.— To further characterize surface processes on the performance of infiltrated LSF-YSZ electrodes, we examined the effect of depositing Al_2O_3 blocking layers over the electrode by ALD. Because ALD can be used to form conformal surface layers over porous surfaces at relatively low temperatures,[36–41] 423 K in this case, there should be no mixing of the Al_2O_3 into the LSF bulk during Al_2O_3 deposition. Therefore, only surface processes should be affected by the presence of the Al_2O_3 layers. Al_2O_3 was chosen because it is expected to act primarily as a physical blocker of electrochemical reactions on the surface of the perovskite, and not form a chemical compound with the LSF or act as a catalyst for O_2 adsorption.[24] As an added benefit, the deposition of Al_2O_3 using trimethyl aluminum (TMA) and water as precursors is one of the most thoroughly characterized ALD systems.[36,39] The reaction between TMA and the substrate is rapid and has been shown to work well on a large number of different substrates.[39]

The films were deposited by alternating exposures to water and TMA (Cambridge Nanotech) using a commercially available system (Savannah 200, Cambridge Nanotech). The reactants were maintained at room temperature, resulting in vapor pressures of about 20 Torr and 11 Torr, respectively, inside the sample containers.[41] The deposition chamber was maintained at 423 K and at a base pressure of 0.08 Torr with a N_2 flow of 5 mL/min. Each deposition cycle consisted of the following steps: 1) stop N_2 flow, 2) pulse water for 15 ms, 3) wait 25 s to achieve uniform coverage throughout the porous sample, 4) purge chamber with N_2 for 10 s, 5) stop N_2 flow, 6) pulse TMA for 15 ms, 7) wait 25 s, 8) purge chamber with N_2 for 10 s. Increasing the duration of steps 3 and 7 to 50 s did not affect the amount deposited per cycle, suggesting that 25 s reaction time was enough to achieve uniform deposition throughout the porous LSF-YSZ electrode. After electrochemical testing, the silver current collectors were carefully removed and the same cells were subject to another series of TMA/water treatments.

The amount of Al_2O_3 deposited by ALD was quantified gravimetrically. The measurements were performed using porous YSZ slabs, 10 × 3 × 3 mm in size, that were prepared from the same slurry used for the preparation of the porous electrodes. The slabs were infiltrated with LSF to a weight loading of 35 wt% and calcined to 1123 K for 4 hours. The specific surface area of each infiltrated slab was determined from Brunauer-Emmett-Teller (BET) isotherms to be 1.75 m^2/g using Kr adsorption at 77 K.[42] The weight of the infiltrated slabs was then measured as a function of the number of ALD cycles. These gravimetric measurements indicated that the Al_2O_3 coverage increased linearly between 1 and 50 cycles, by 1.1 Al atoms/nm^2 per cycle. This corresponds to a surface coverage of roughly 10% of a monolayer per cycle.

An estimate of the fraction of the LSF remaining uncovered following a given number of Al_2O_3 deposition cycles was also determined using NO_2 titrations. The hypothesis behind this technique is that NO_2 reacts with oxygen vacancies on the LSF surface to form NO and fill the vacancy, and that surface sites covered by Al_2O_3 would not be reactive. For these experiments, we prepared a pellet made from LSF powder synthesized from the same nitrate/citric acid solution that was used to prepare electrodes by infiltration. After removing the water from the solution and heating the remaining solid to 973 K for 4 hours, the resulting LSF powder was pressed into disks, 1 mm in thickness, and then calcined to 1123 K for 4 h. The specific surface area of this material was determined to be 5.2 m^2/g using the BET isotherms. Between 0.72 and 0.75 g of the LSF wafers were loaded into a quartz-tube flow reactor and flushed with dry He (Ultra High Purity grade, Airgas) for 1 h at 723 K using a flow rate of 10.5 mL/min. After cooling the sample to 473 K, the He gas stream was changed to a stream of 5.1% of NO_2 in He (Airgas) while monitoring the mass spectra of the outlet gases.

As shown in Figure 1a, NO_2 (mass-to-charge ratio, $m/z = 30, 46$) is unaffected by heating in the empty reactor. When unmodified LSF wafers are placed in the reactor, Figure 1b, only NO ($m/z = 30$) was observed leaving the reactor initially but this changed to NO_2 ($m/z = 30, 46$) after all of the surface vacancy sites had been consumed.

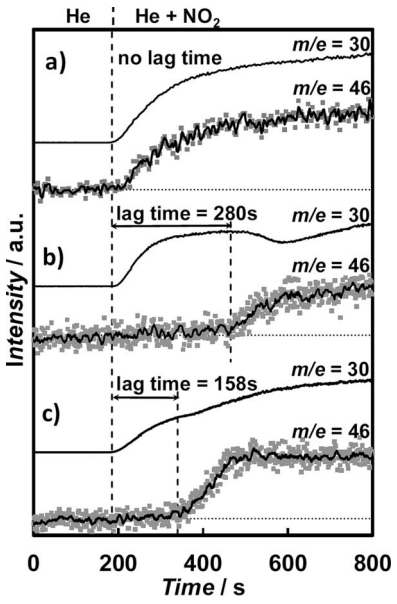

Figure 1. NO_2 flow titration results for a) an empty reactor, b) pure LSF, and c) the same LSF sample as in b) but coated with 20 cycles of Al_2O_3. The titration was carried out at 473 K. NO_2 reacts with vacancies in the LSF surface, producing NO signal ($m/z = 30$). The lag for the onset of the NO_2 ($m/z = 46$) signal is a measure of the vacancy site concentration.

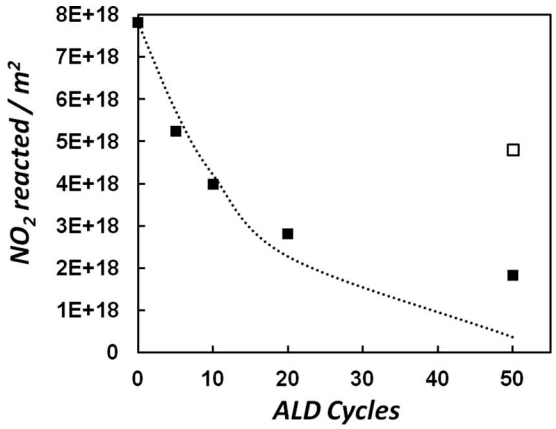

Figure 2. The specific vacancy concentration in LSF as a function of the number of Al_2O_3 ALD cycles that were deposited at 423 K, as determined by NO_2 flow titration. The dashed line is an empirical fit to the experimental data assuming the growth proceeds via the random deposition model[38] with a per-cycle coverage of 6%. The open symbol was obtained on the Al_2O_3-coated LSF after heating in air to 1073 K for 4 h.

The lag time between the observations of NO and NO_2, 280 s in this example, was then used to calculate the number of sites that were titrated. The results in Figure 1c show that the lag time decreased significantly after 20 Al_2O_3 ALD cycles had been added to the LSF.

The change in the concentration of LSF oxygen vacancy sites as a function of the number of ALD cycles is shown in Figure 2. The exponential decrease in the site density with the number of ALD cycles suggests that the growth of Al_2O_3 on LSF proceeds via random deposition over the entire surface.[39] Fitting the data in Figure 2 to such a model indicates that, on average, just 6% of the LSF surface is covered per cycle, implying that, even after 20 cycles, roughly a third of the surface remains exposed and potentially electrochemically active.

Results

Effect of calcination temperature on LSF-YSZ composite.— Previous studies have shown that the calcination temperature used to prepare the infiltrated LSF electrodes has a strong impact on the structure and surface area of the LSF phase and that the changes in turn strongly affect electrode performance.[4,7–9,27,28,31–34] The changes in microstructure are demonstrated by the SEM micrographs of LSF-YSZ composites after calcination to 1123 K and 1373 K, presented in Figure 3. For the 1123 K sample, the LSF particles are small, with a characteristic size of about 50 nm, and appear to coat the YSZ channels uniformly. The regions in the image without fine particles correspond to the YSZ fracture surfaces. After calcination to 1373 K, the microstructure changes dramatically and the LSF phase now appears to form a dense film over the YSZ scaffold. The BET surface areas of 35-wt% LSF-YSZ composites also showed a dependence on calcination temperature. After calcination to 1123 K, the surface area was 1.75 m^2/g; this decreased to 0.48 m^2/g after calcination to 1373 K. Interestingly, the surface area of the composite after treatment at 1373 K is similar to that of the empty YSZ scaffold, corroborating the fact that the LSF forms a dense film at this temperature.

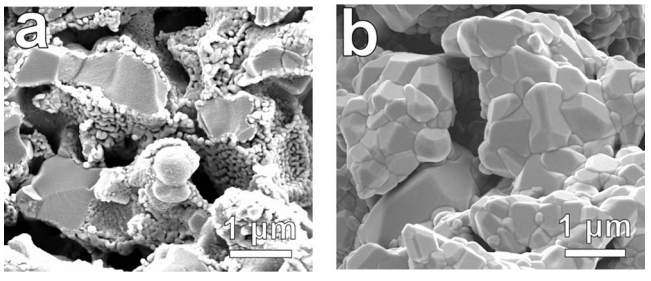

Figure 3. Scanning electron microscopy images of LSF-YSZ electrodes prepared by infiltration after calcination to (a) 1123 K and (b) 1373 K. In (a), the YSZ fracture surfaces are visible as gray areas without perovskite particles. In (b), the LSF phase uniformly covers the YSZ, and distinction between phases is difficult.

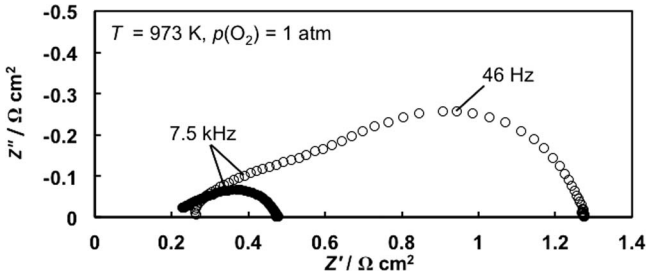

Figure 4. Nyquist plots of LSF-YSZ cathode symmetric cells measured at 973 K in pure O_2. The two sets of data correspond to cells calcined to 1123 K (closed symbols) and 1373 K (open symbols).

Figure 4 summarizes the electrochemical properties for the electrodes with the structures shown in Figure 3. The measurements were conducted using LSF-YSZ symmetric cells at 973 K in pure oxygen atmosphere and the impedances have been divided by two to account for the presence of two electrodes. The non-ohmic impedance of the cell calcined to only 1123 K was significantly lower than that of the cell calcined to 1373 K, 0.24 $\Omega \cdot cm^2$ versus 1.0 $\Omega \cdot cm^2$; however, the corresponding ohmic resistances shown in Figure 4 were nearly the same, 0.23 $\Omega \cdot cm^2$ and 0.25 $\Omega \cdot cm^2$, and very close to half that expected for a 80 μm YSZ film, 0.23 $\Omega \cdot cm^2$ at 973 K.[43] The non-ohmic part of the spectrum for the 1123-K cell is dominated by single arc with a characteristic frequency of 7.5 kHz, although a much smaller high frequency arc may also be present. For the purposes of this study, we assume that the impedance is primarily due to a single process with a resistance, R_p. In contrast, at least two processes with very different time constants are readily apparent in the spectrum of the 1373-K electrode. Since LSF does not react with YSZ at 1373 K[27,28] and the YSZ scaffold, sintered to 1773 K, is microstructurally stable under these conditions, all changes in electrode performance can be related to changes in the microstructure of the LSF phase, as discussed elsewhere.[3,4,27,32]

$p(O_2)$ dependence of LSF-YSZ electrodes.— In order to understand the origin of the features in the impedance spectra in Figure 4, we measured impedance spectra for both cells as a function of the $p(O_2)$, with results shown in Figure 5. For the cell calcined at 1123 K, the non-ohmic impedance (Figure 5a) increased from 0.24 $\Omega \cdot cm^2$ in 1

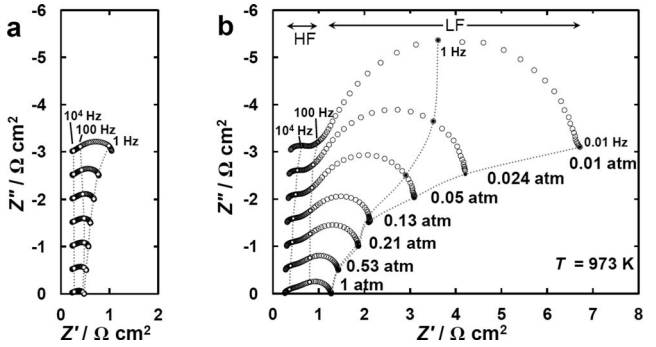

Figure 5. Nyquist plots of LSF-YSZ symmetric cells measured at 973 K as a function of oxygen partial pressure: (a) LSF-YSZ calcined to 1123 K, (b) LSF-YSZ calcined to 1373 K. The impedance spectra have been offset in Z'' for clarity. The spectra in (a) were measured at the same $p(O_2)$ as in (b).

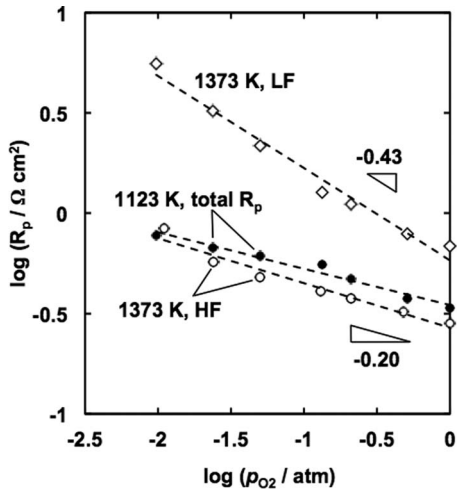

Figure 6. The O_2 partial pressure dependence of processes in the impedance spectra of LSF-YSZ electrodes at 973 K: (●) total electrode polarization resistance of a cell calcined at 1123 K, (o) the high-frequency (HF) polarization resistance of a cell heated to 1373 K, and (◊) low-frequency (LF) polarization resistance of a cell heated to 1373 K.

atm O_2 to 0.81 $\Omega \cdot cm^2$ in 0.01 atm O_2. While there was some shift in the relative position of representative frequencies on the Nyquist plot, there were no dramatic changes in the shape of the spectra with pressure.

In contrast to the results for the 1123-K composite, the Nyquist plot for the 1373-K electrode changed significantly with decreasing $p(O_2)$. First, the ohmic component increased from 0.25 $\Omega \cdot cm^2$ at $p(O_2) = 1$ atm to 0.39 $\Omega \cdot cm^2$ at $p(O_2) = 0.01$ atm, implying that there was a decrease in the conductivity of the LSF-YSZ.[10,31] The increased ohmic resistance is observed here because the conductivity of LSF-YSZ electrodes prepared by infiltration are lower following calcination to 1373 K.[31] Second, there was a significant change in the shape of the non-ohmic part of the Nyquist plots with decreasing $p(O_2)$. As noted above, there are at least two arcs in the spectrum for the 1373-K composite, corresponding to low (LF) and high (HF) frequency processes, with the LF feature gaining in prominence with decreasing $p(O_2)$. To quantify the effect of $p(O_2)$ on the impedance, the lengths of the LF and HF arcs were extracted from the spectra using a simple $R_\Omega(R_{HF}Q_{HF})(R_{LF}Q_{LF})$ circuit. Here, R_Ω stands for the ohmic resistance, R_{HF} and R_{LF} are the impedances associated with the HF and LF process, and Q_{HF} and Q_{LF} are the corresponding constant phase elements.[44]

Figure 6 is a plot of the resistances extracted from Figure 5 as a function of $p(O_2)$ on a log-log scale. The resistances for the 1123-K composite, R_p, and the high-frequency component of the 1373-K composite, R_{HF}, exhibited a relatively weak $p(O_2)$ dependence, $p(O_2)^{-0.22}$ for R_{HF}, and $p(O_2)^{-0.17}$ for R_p. The similarities in both the absolute values of R_{HF} and R_p and in their $p(O_2)$ dependences strongly suggest that these resistances are associated with the same processes. In contrast, R_{LF} for the 1373-K composite exhibited a much stronger dependence, being proportional to $p(O_2)^{-0.43}$. While low-frequency electrode processes are often assumed to be associated with gas-phase diffusion limitations for anode supported cells with very thick electrodes, this is unlikely to be the case here. Although the $p(O_2)$ dependence for a process limited by gas-phase diffusion could be −0.5 depending on the relative importance of Knudsen and molecular diffusion, diffusion limitations should be more important for the 1123-K composite due to its higher surface area and smaller pore structure. The absence of a low-frequency resistance for the 1123-K composite, therefore, argues against diffusion limitations making a significant contribution to the impedance spectra for these electrodes. Instead, we propose that the $p(O_2)^{-0.5}$ dependence is associated with dissociative adsorption of molecular O_2 on the perovskite surface being the rate limiting step. This conclusion is consistent with previous results reported in the literature.[8,10,45]

Additional information on the nature of the limiting electrode processes was obtained from impedance measurements with the symmetric cells at a $p(O_2)$ of 0.05 atm, with an imposed current density of 100 mA/cm^2. The results for the 1123-K and 1373-K electrodes are shown in Figure 7. Obviously, the cells are no longer symmetric under these conditions, since one of the electrodes will be polarized anodically and the other cathodically. For the 1123-K electrodes, the impedance arcs were unaffected by the application of current (Figure 7a), implying that charge-transfer steps are not rate limiting. The high-frequency arc in the impedance spectrum of the 1373-K electrode was similarly unaffected by the imposed current (Figure 7b). We suggest that the limiting process corresponding to these two HF resistances is the diffusion of oxygen ions within the LSF phase, since ion diffusion is expected to be independent of the applied current and weakly dependent on $p(O_2)$.[46] This conclusion is supported by a mathematical model of composite cathodes, developed by Bidrawn et al. in Ref. 8, that suggests infiltrated electrodes are typically limited by O_2 adsorption except when the infiltrated perovskite has a very low ion conductivity. In contrast, the low-frequency resistance in the spectrum of the 1373-K cell decreases dramatically with applied current. This is again consistent with the LF process being associated with surface reactions, since electrode polarization will alter the concentration of vacancies within the perovskite, which in turn affects the rates of O_2 adsorption and desorption.[8]

To summarize the conclusions from studies of $p(O_2)$ dependence, LSF-YSZ composites that have been prepared by infiltration methods and calcined to only 1123 K exhibit a dominant, high-frequency arc in their impedance spectrum. The resistance associated with this arc is weakly dependent on $p(O_2)$, unaffected by applied currents, and likely results from diffusion of oxygen ions within the perovskite phase. Calcination of these same LSF-YSZ composites to 1373 K results in microstructural changes in the LSF phase that are responsible for an additional, low-frequency arc in the corresponding impedance spectra. The resistance corresponding to this arc is due to adsorption limitations on the perovskite surface.

Inert Al_2O_3 blocking layers.— Impedance measurements were performed on symmetric cells as a function of the number of ALD cycles. As discussed in the Experimental section, both gravimetric and NO_2-titration measurements indicated that roughly 6 to 10% of the LSF

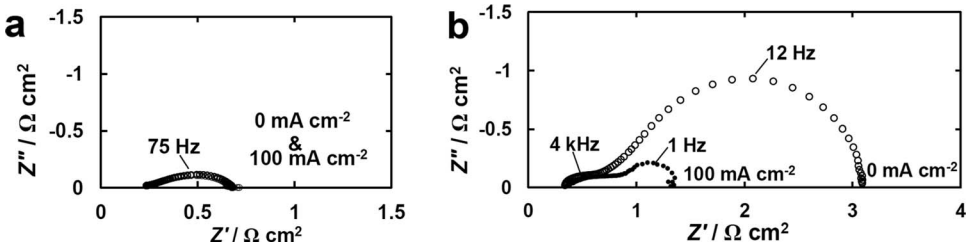

Figure 7. Nyquist plots of LSF-YSZ symmetric cells measured at 973 K in 5% O_2-Ar mixtures as a function of applied current density: (a) LSF-YSZ calcined to 1123 K, (b) LSF-YSZ calcined to 1373 K.

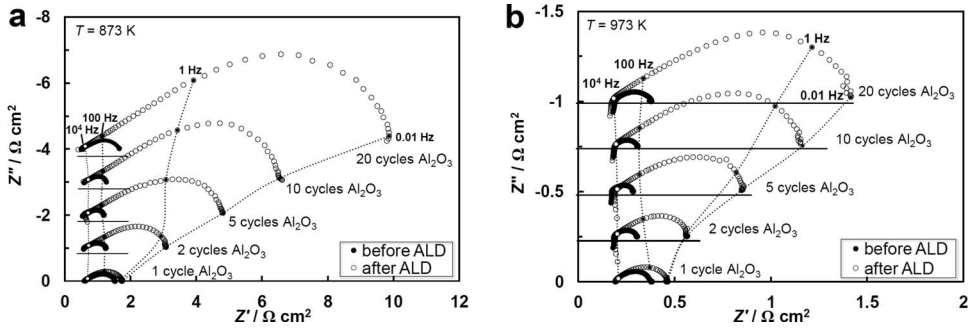

Figure 8. Nyquist plots of LSF-YSZ cathode symmetric cells calcined to 1123 K and measured at 873 K before and after ALD treatment. The impedance spectra have been offset in Z'' for clarity.

surface was covered by Al_2O_3 with each ALD cycle. Because there was evidence that the Al_2O_3 film broke up at higher temperatures, initial experiments were carried out at 873 K before proceeding to higher temperatures.

The impedance spectra, measured in air at 873 K on 1123-K, LSF-YSZ composite electrodes, are shown in Figure 8 as a function of the number of ALD cycles deposited. To ensure that the changes were caused by the addition of Al_2O_3, impedance spectra were acquired on each cell used for the data in Figure 8 prior to adding Al_2O_3. The silver current collectors were then carefully removed and the cells exposed to a given number of ALD cycles before the electrochemical performance was again tested at 873 K. As expected, the addition of Al_2O_3 blocking layers was found to adversely affect cell performance in a manner that increased with the number of ALD cycles to which the electrode was exposed. At 873 K (Figure 8a), the electrode impedances increased from $0.8 \pm 0.2\ \Omega \cdot cm^2$, to $1.1\ \Omega \cdot cm^2$ (after 1 cycle of Al_2O_3), $2.5\ \Omega \cdot cm^2$ (2 cycles of Al_2O_3), $4.2\ \Omega \cdot cm^2$ (5 cycles of Al_2O_3), $6.0\ \Omega \cdot cm^2$ (10 cycles of Al_2O_3), $9.4\ \Omega \cdot cm^2$ (20 cycles of Al_2O_3), and $24.5\ \Omega \cdot cm^2$ (50 cycles of Al_2O_3, not shown). The only surprise in these results is that the increase in the impedances was greater than the fraction of the surface that was covered. Measurements performed at 973 K on these same cells, shown in Figure 8b, showed proportionally similar effects, with electrode resistances increasing from $0.15 \pm 0.04\ \Omega \cdot cm^2$ to $0.26\ \Omega \cdot cm^2$ (after 1 cycle of Al_2O_3), $0.36\ \Omega \cdot cm^2$ (2 cycles of Al_2O_3), $0.65\ \Omega \cdot cm^2$ (5 cycles of Al_2O_3), $0.95\ \Omega \cdot cm^2$ (10 cycles of Al_2O_3), $1.25\ \Omega \cdot cm^2$ (20 cycles of Al_2O_3), and $2.0\ \Omega \cdot cm^2$ (50 cycles of Al_2O_3, not shown) at 973 K.

However, when the cells used in taking the data in Figure 8 were heated to 1073 K, the effects of Al_2O_3 addition decreased dramatically and remained low, even after cooling the cell back to 973 K. Figure 9 shows impedance spectra at 973 K in air for the cell with 5 ALD cycles, before and after heating to 1073 K. The impedance of the cell with Al_2O_3 addition did not revert back completely to the original value, but it did decrease from $0.65\ \Omega \cdot cm^2$ to $0.20\ \Omega \cdot cm^2$. This observation is consistent with the results shown in Figure 2 (open symbol), where an increase in free oxygen vacancy sites was observed after heating the LSF coated with 50 cycles of Al_2O_3 to 1073 K. These results provide strong evidence that the deactivation associated with the addition of Al_2O_3 at lower temperatures is due to physical blocking of the surface, since one might expect electrode deactivation to be more pronounced after heating if deactivation were due to a chemical process, such as reaction between Al_2O_3 and LSF.[24] Assuming that deactivation is due to physical blocking of the surface by Al_2O_3, the performance recovery at 1073 K likely results from the Al_2O_3 film breaking up due to thermally induced mechanical stresses. In Figures 8 and 9, it is also important to notice the characteristic frequencies shift to lower values in the electrodes deactivated by Al_2O_3. In previous sections of this paper, it was shown that adsorption-rate limitations are associated with low-frequency processes. The adsorption rate must certainly be affected by adding Al_2O_3 layers to the LSF surface. The changes in the characteristic frequencies are consistent with that conclusion and provide further evidence that the low-frequency processes are associated with adsorption.

We also examined the effect of current on the Al_2O_3-coated electrodes at 873 K, with results for a cell with 50 ALD layers summarized in Figure 10. In these experiments, current was passed in both directions so that both electrodes of the symmetric cell would experience identical conditions. The electrodes had an initial non-ohmic impedance of $24.5\ \Omega \cdot cm^2$ at zero current. After the application of $14\ mA/cm^2$ for 15 min in each direction, the total polarization resistance decreased by more than 40% to $14.4\ \Omega \cdot cm^2$. Further decreases in the resistance were observed as the magnitude of the current increased, reaching a minimum less than 20% of the initial impedance. It should be noted that LSF electrodes prepared by infiltration and calcination to 1123 K are not susceptible to polarization activation, as is

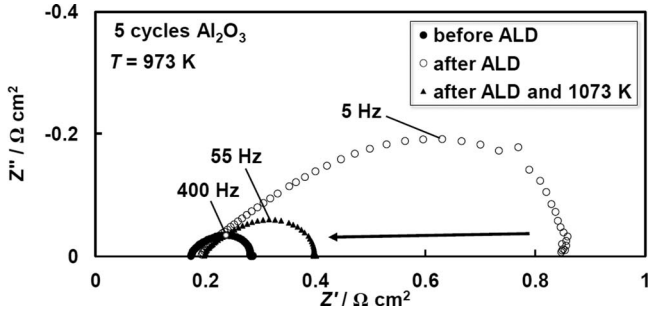

Figure 9. Nyquist plots of LSF-YSZ cathode symmetric cells calcined to 1123 K and tested at 973 K, before and after a 5-cycle Al_2O_3 ALD. Performance is partly restored after the ALD layer disintegrates because of heating to 1073 K.

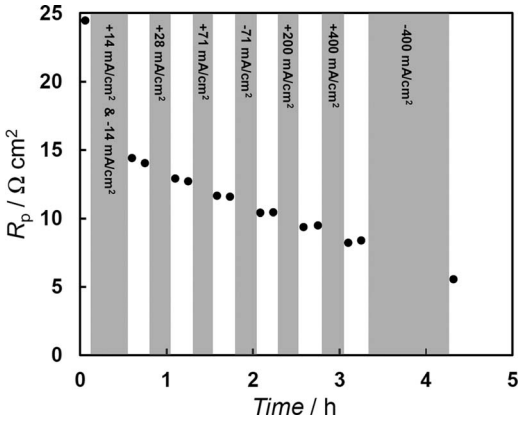

Figure 10. Electrode polarization resistance for an LSF-YSZ symmetric cell, calcined to 1123 K and coated with 50 ALD cycles of Al_2O_3, measured at zero current (white regions) at 873 K, as a function of current load (the load was applied immediately before the measurements (gray regions)).

commonly observed for materials such as Sr-doped $LaMnO_3$ [9,30,47,48] or $LaNi_{0.6}Fe_{0.4}O_3$.[34] Furthermore, the final resistance in Figure 10 did not increase again with time over a period of at least 24 h.

We attribute the observed changes in impedance with current to the breaking up of the conformal alumina film, caused by the partial reduction and restructuring of the LSF surface upon the application of current. These observations agree well with the recent results of Mutoro et al., who showed that the surface composition of perovskite materials, such as $La_{0.8}Sr_{0.2}CoO_3$, changes significantly with electrical potential.[49] This is evidence that the perovskite surfaces used for SOFC electrodes can be restructured both thermally and electrochemically.

Discussion

There are several interesting implications that can be drawn from this study about LSF-YSZ electrodes prepared by infiltration methods. Based on the studies of $p(O_2)$ dependence on electrode performance, there appear to be two sets of processes, one set of high-frequency processes associated with diffusion of ions within the electrode and one set of low-frequency processes associated with dissociative adsorption of gas-phase O_2 onto the perovskite surface. Depending on the surface area of the perovskite phase, one set of processes or the other can dominate the electrode performance. Calcination to higher temperatures decreases the surface area of the LSF phase, causing O_2 adsorption to be limiting. This is in agreement with conclusions from previous studies where the surface areas of both the LSF and perovskite scaffold were varied.[7,8,31]

It has been shown here and in other studies that the resistance of the processes we are associating with gas-phase adsorption decreases dramatically with applied current, both anodic and cathodic.[9,27,29–32,34,48] With cathodic polarization for an electrode that is limited by adsorption of O_2, the perovskite surface will be reduced, causing an increase in the vacancy site concentration.[8] Since O_2 adsorption should be proportional to the concentration of vacancies, a decreased resistance is to be expected. However, the opposite should be expected for anodic polarization. We can only speculate as to why anodic polarization also decreases the resistance but it may be that new sites on the perovskite become accessible at the higher $p(O_2)$. For example, one often observes a shift in the redox isotherm for perovskites like $La_{(1-x)}Sr_xFeO_{(3-x/2)}$, from oxygen stoichiometries of (3−x/2) to 3, in the higher $p(O_2)$ range.[50] Since the oxygen-exchange rate is the difference between the adsorption and desorption rates, population of these added sites could be important.

Several conclusions can also be reached from the ALD studies. First, any loss of LSF surface area, whether the loss is due to high-temperature sintering or to surface blocking by Al_2O_3, leads to increased electrode resistance. The performance of LSF-YSZ cathodes depends strongly on the availability of the perovskite surface within the electrode. As an increasing fraction of the surface becomes unavailable, either by being coated with an inactive species or through sintering, the surface-related, low-frequency surface process becomes increasingly more dominant. Furthermore, the impedance spectra collected after thermal deactivation and after an ALD treatment are very similar in shape and characteristic frequency.

It is interesting to compare the effect of decreasing the LSF surface area by covering it with Al_2O_3 to the effect of decreasing the LSF surface area by thermal sintering. In a previous publication,[7] our lab reported the resistance of LSF-YSZ, prepared by identical methods to that used in the present study, as a function of the surface area of the electrode, varying the surface area by changing the calcination temperature. These data are reproduced in Figure 11, together with the present data for 1123-K LSF-YSZ electrodes modified by ALD. With the ALD-modified electrodes, the electrode resistance is plotted as a function of the fraction of available sites, determined by NO_2 titration. While absolute comparisons are difficult, the plot does show remarkable similarities in the trends for the two sets of data. In both cases, the relationship between the availability of the LSF surface and performance is non-linear, and the polarization resistance increases

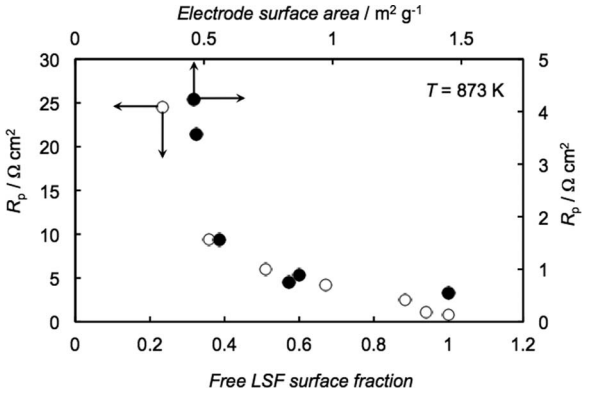

Figure 11. The polarization resistance, R_p, of LSF-YSZ cathodes heated to 1123 K and coated with a thin coating of alumina as a function of the available LSF surface fraction, as determined by NO_2 flow titration experiments (open symbols). The relationship between LSF-YSZ electrode surface area and R_p from Ref. 7 is given on the other two axes (closed symbols). The electrode with a surface area of 1.45 m^2/g was identical to LSF-YSZ electrodes used in this study and was also calcined to 1123 K. All data were acquired at 873 K under no current load.

dramatically after about a third of the initial LSF surface is covered or lost due to sintering. The difference in the absolute magnitude of the resistance is to be expected since the minimum achievable surface area is set by the surface area of the underlying YSZ backbone when the surface is decreased by thermal treatments.[32]

Since the temperatures at which ALD was carried out are too low to result in any degree of Al_2O_3 incorporation into the bulk of the perovskite phase, the deposited alumina can only affect processes occurring on the immediate surface of LSF. This implies that the electrochemically inactive oxide coating effectively modifies the net rate of oxygen adsorption onto the LSF surface. Some of us have previously argued that it is useful to use the flux of gaseous O_2 molecules to the surface, as determined by the Kinetic Theory of Gases, along with a reactive sticking coefficient (i.e. the probability that an oxygen molecule hitting the perovskite surface will adsorb) to express the adsorption rate, r_{ads}, of O_2 on the electrode:[8]

$$r_{ads} = \frac{p(O_2)}{\sqrt{2\pi MRT}} \cdot S. \qquad [1]$$

In this equation, M is the molecular weight of O_2, R is the universal gas constant, T is temperature, and S is the sticking coefficient. Since oxygen adsorption is likely to occur at surface oxygen vacancy sites, it is expected that S will be proportional to the surface vacancy concentration, so that

$$S = S_0 \cdot \frac{[V_O^{\bullet\bullet}]}{[O_{surf}]}. \qquad [2]$$

Here, S_0 is the probability of adsorption on a vacancy site and $\frac{[V_O^{\bullet\bullet}]}{[O_{surf}]}$ is the fraction of the surface that is vacancies.[8] This approach is consistent with previous studies that have shown that the surface-exchange rates correlate with vacancy concentrations.[51] Note that since S is a probability, it must have value between 0 and 1.

The resistance of composites electrodes, R_p, having a structure similar to that used in the present study has been calculated in terms S_0.[8]

$$R_p = \frac{k}{(1-p)}\sqrt{\frac{3/2w\tau}{p(O_2)\cdot m \cdot S_0 \cdot \sigma_{YSZ}}}, \qquad [3]$$

where $k = 0.0256\ \Omega^{\frac{1}{2}}\ Pa^{\frac{1}{2}}$ cm (at 873 K), p is porosity of the electrode, w is the characteristic length-scale of the electrolyte scaffold, τ is tortuosity for ion conduction, m is the reducibility constant of the perovskite material (defined as the slope of the plot of 3-δ vs log $p(O_2)$), and σ_{YSZ} is the ionic conductivity of the porous YSZ

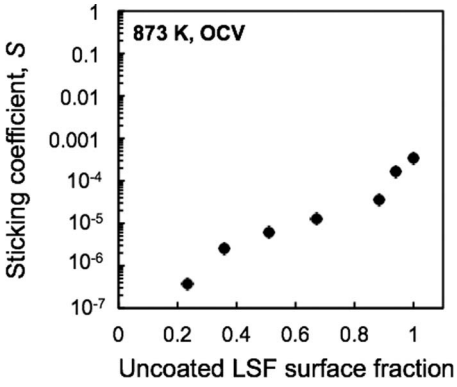

Figure 12. Sticking coefficient on a vacancy site, S_0, plotted as a function of the availability of the LSF surface (as determined from flow titration experiments).

electrolyte (see Ref. 8 for details). Based on the relationship between the polarization resistance and the sticking coefficient in Equation 3, the blocking effect of Al_2O_3 can be quantified on the atomic level, as shown in Figure 12. According to the data, deposited coatings decrease the probability of oxygen adsorption onto the electrode surface, with the sticking coefficient after 50 ALD cycles (corresponding to an LSF surface availability of 0.24) being almost three orders of magnitude lower than that of an untreated LSF-YSZ sample.

There are various possibilities as to why the sticking probability would not decrease linearly with Al_2O_3 coverage. For example, Equation 3 does not account for the fact that dissociative adsorption requires a pair of vacancy sites for the adsorption of O_2. However, the logarithmic dependence in Figure 12 is still much stronger than the square dependence that would be expected for dissociative adsorption. Figure 12 suggests that each alumina species has a more long-ranging effect on electrode performance, possibly by modifying the energetics of neighboring sites.

Obviously, there is still much to learn about the processes responsible for the electrode impedances of perovskite-YSZ composites. However, we suggest that the tools discussed in this paper help provide insights into those processes.

Conclusions

Increases in the SOFC electrode resistances of LSF-YSZ composites caused by changes in the surface area of the LSF due to sintering were related to changes caused by Al_2O_3 overlayers. In both cases, the losses in LSF surface area cause increases in the electrode resistance by limiting O_2 adsorption. The processes associated with O_2 adsorption are shown to have low characteristic frequencies that have sometimes been interpreted as resulting from diffusion limitations. Finally, the use of ALD overlayers on the electrode was used to show that the LSF film undergoes structural changes upon polarization.

Acknowledgments

This work was funded by the U.S. Department of Energy's Hydrogen Fuel Initiative (Grant no. DE-FG02-05ER15721). R.K. also acknowledges the financial support of the U.S. Department of State under the auspices of the International Fulbright Science & Technology Award.

References

1. S. Singhal and K. Kendall (Eds.), *High temperature solid oxide fuel cells: fundamentals, design and applications*, Elsevier, Oxford, 2003.
2. R. O'Hayre, S.-W. Cha, W. Collela, and F. B. Prinz (Eds.), *Fuel Cell Fundamentals*, 2nd Ed., Wiley, Hoboken, 2009.
3. J. M. Vohs and R. J. Gorte, *Adv. Mat.*, **21**, 943 (2009).
4. F. Bidrawn, S. Lee, J. M. Vohs, and R. J. Gorte, *J. Electrochem. Soc.*, **155**(7), B660 (2008).
5. S. B. Adler, *Chem. Rev.*, **104**, 4791 (2004).
6. V. A. C. Haanappel, N. Jordan, A. Mai, J. Mertens, J. M. Serra, F. Tietz, S. Uhlenbruck, I. C. Vinke, M. J. Smith, and L. G. J. de Haart, *J. Fuel Cell Sci. Tech.*, **6**, 021302 (2009).
7. R. Küngas, F. Bidrawn, E. Mahmoud, J. M. Vohs, and R. J. Gorte, *Solid State Ionics*, **225**, 146 (2012).
8. F. Bidrawn, R. Küngas, J. M. Vohs, and R. J. Gorte, *J. Electrochem. Soc.*, **158**(5), B514 (2011).
9. F. Bidrawn, N. Aramrueang, J. M. Vohs, and R. J. Gorte, *J. Power Sources*, **195**, 720 (2010).
10. M. Mosleh, M. Søgaard, and P. V. Hendriksen, *J. Electrochem. Soc.*, **156**(4), B441 (2009).
11. E. N. Armstrong, K. L. Duncan, D. J. Oh, J. F. Weaver, and E. D. Wachsman, *J. Electrochem. Soc.*, **158**(5), B492 (2011).
12. J. A. Kilner, R. A. De Souza, and I. C. Fullarton, *Solid State Ionics*, **86–88**, 703 (1996).
13. A. Endo, H. Fukunaga, C. Wen, and K. Yamada, *Solid State Ionics*, **135**, 353 (2000).
14. A. Endo, S. Wada, C.-J. Wen, H. Komiyama, and K. Yamada, *J. Electrochem. Soc.*, **145**(3), L35 (1998).
15. S. B. Adler, *Solid State Ionics*, **111**, 125 (1998).
16. S. P. Jiang, *Int. J. Hydrogen Energy*, **37**, 449 (2012).
17. F. L. Liang, J. Chen, S. P. Jiang, B. Chi, J. Pu, and L. Jian, *Electrochem. Solid- State Lett.*, **11**, B213 (2008).
18. S. P. Jiang and W. Wang, *J. Electrochem. Soc.*, **152**, A1398 (2005).
19. N. Ai, S. P. Jiang, Z. Lü, K. Chen, and W. Su, *J. Electrochem. Soc.*, **157**(7), B1033 (2010).
20. T. Z. Sholklapper, C. P. Jacobsen, S. J. Visco, and L. C. De Jonghe, *Fuel Cells*, **8**(5), 303 (2008).
21. X. Lou, S. Wang, Z. Liu, L. Yang, and M. Liu, *Solid State Ionics*, **180**, 1285 (2009).
22. C. Knöfel, H.-J. Wang, K. T. S. Thydén, and M. Mogensen, *Solid State Ionics*, **195**, 36 (2011).
23. M. Mogensen, M. Søgaard, P. Blennow, and K. Kammer Hansen, *Proc. 8. European SOFC Forum*, Lucerne, Switzerland, 2008, 6 p.
24. K. Kammer Hansen, M. Wandel, Y.-L. Liu, and M. Mogensen, *Electrochim. Acta*, **55**, 4606 (2010).
25. C. W. Tanner, K.-Z. Fung, and A. V. Virkar, *J. Electrochem. Soc.*, **144**, 21 (1997).
26. J. D. Nicholas and S. A. Barnett, *J. Electrochem. Soc.*, **156**(4), B458 (2009).
27. W. Wang, M. D. Gross, J. M. Vohs, and R. J. Gorte, *J. Electrochem. Soc.*, **154**(5), B439 (2007).
28. L. Adijanto, R. Küngas, F. Bidrawn, R. J. Gorte, and J. M. Vohs, *J. Power Sources*, **196**, 5797 (2011).
29. R. Küngas, F. Bidrawn, J. M. Vohs, and R. J. Gorte, *Electrochem. Solid-State Lett.*, **13**, B87 (2010).
30. Y. Huang, J. M. Vohs, and R. J. Gorte, *J. Electrochem. Soc.*, **152**(7), A1347 (2005).
31. Y. Huang, J. M. Vohs, and R. J. Gorte, *J. Electrochem. Soc.*, **151**(4), A646 (2004).
32. R. Küngas, J.-S. Kim, J. M. Vohs, and R. J. Gorte, *J. Am. Ceram. Soc.*, **94**(7), 2220 (2011).
33. R. Küngas, J. M. Vohs, and R. J. Gorte, *J. Electrochem. Soc.*, **158**(6), B743 (2011).
34. S. Lee, M. Bevilacqua, P. Fornasiero, J. M. Vohs, and R. J. Gorte, *J. Power Sources*, **193**, 747 (2009).
35. R. J. Gorte and J. M. Vohs, *Annu. Rev. Chem. Biomol. Eng.*, **2**, 9 (2011).
36. R. L. Puurunen and W. Vandervorst, *J. Appl. Phys.*, **96**, 7686 (2004).
37. T. Suntola, *Thin Solid Films*, **216**, 84 (1992).
38. M. Cassir, A. Ringuedé, and L. Niinistö, *J. Mater. Chem.*, **20**, 8987 (2010).
39. R. L. Puurunen, *J. Appl. Phys.*, **97**, 121301 (2005).
40. R. L. Puurunen, *Chem. Vap. Deposition*, **9**(5), 249 (2003).
41. R. A. Wind and S. M. George, *J. Phys. Chem. A*, **114**, 1281 (2010).
42. D. Wang, Y. Kang, V. Doan-Nguyen, J. Chen, R. Küngas, N. Wieder, K. Bakhmutsky, R. J. Gorte, and C. B. Murray, *Angew. Chem.*, **50**(19), 4378 (2011).
43. V. V. Kharton, F. M. B. Marques, and A. Atkinson, *Solid State Ionics*, **174**, 135 (2004).
44. J. R. Macdonald and W. B. Johnson, in: E. Barsoukov and J. R. Macdonald (eds.), *Impedance Spectroscopy: Theory, Experiment, and Applications*, 2nd Ed., John Wiley & Sons, Hoboken, USA, 2005, p. 18.
45. Y. Takeda, R. Kanno, M. Noda, Y. Tomida, and O. Yamamoto, *J. Electrochem. Soc.*, **134**(11), 2656 (1987).
46. B. A. van Hassel, T. Kawada, N. Sakai, H. Yokokawa, M. Dokiya, and H. J. M. Bouwmeester, *Solid State Ionics*, **66**, 295 (1993).
47. S. P. Jiang, *J. Solid State Electrochem.*, **11**, 93 (2007).
48. S. McIntosh, S. B. Adler, J. M. Vohs, and R. J. Gorte, *Electrochem. Solid-State Lett.*, **7**(5), A111 (2004).
49. E. Mutoro, E. J. Crumlin, H. Pöpke, B. Luerssen, M. Amati, M. K. Abyaneh, M. D. Biegalski, H. M. Christen, L. Gregoratti, J. Janek, and Y. Shao-Horn, *J. Phys. Chem. Lett.*, **3**, 40 (2012).
50. J. Mizusaki, M. Yoshihiro, S. Yamauchi, and K. Fueki, *J. Solid State Chem.*, **58**, 257 (1985).
51. L. Wang, R. Merkle, and J. Maier, *J. Electrochem. Soc.*, **157**(12), B1802 (2010).